Effect of Injection Zone Cracking on Fluid Catalytic Cracking

Rajesh Patel, Dawei Wang, and Chao Zhu
Dept. of Mechanical and Industrial Engineering, New Jersey Institute of Technology, Newark, NJ 07102

Teh C. Ho
Corporate Strategic Research Laboratories, ExxonMobil Research and Engineering Co., Annandale, NJ 08801

DOI 10.1002/aic.13902
Published online September 26, 2012 in Wiley Online Library (wileyonlinelibrary.com).

Fluid catalytic cracking (FCC) is a refining process for converting heavy oils to valuable products such as gasoline and olefins. Modeling of this process is quite challenging. A common assumption has been that vaporization is instantaneously fast and cracking is negligible in the injection zone. Relaxing this assumption, an approach for quantifying the effect of injection zone cracking on FCC performance is developed. The approach combines a Lagrangian description of the spray behavior with an Eulerian modeling of transport-cracking coupling in the FCC riser. Included in the model are droplet vaporization, a four-lump kinetic network, spray penetration trajectory, solid-fluid and solid-solid collisions, and multispray interactions. Parametric studies show that precracking in the injection zone plays an important role in steering the overall performance of an FCC riser. The model developed here can accommodate a large number of reactions, thus, allowing for composition-based modeling of the FCC process. © 2012 American Institute of Chemical Engineers *AIChE J,* 59: 1226–1235, 2013
Keywords: fluid catalytic cracking riser, vaporizing spray, feed injection, droplet-solid collision

Introduction

Fluid catalytic cracking (FCC), the primary conversion process in oil refining, produces olefins, gasoline, and distillates. It removes sulfur and upgrades residue. In this process the liquid feed enters into the bottom of a riser reactor through multiple atomizers installed circumferentially on the reactor wall, as Figure 1 shows. The issuing liquid jet experiences transverse impingement of the upward flowing catalyst that is extremely hot. The oil drops are vaporized and cracked upon colliding with catalyst particles. After rising through the riser, the catalyst goes through cyclones and a steam stripper. It is then fed to a regenerator to burn off the coke and returns to the riser to complete the circuit. The heat generated in the regenerator is used to vaporize and crack the hydrocarbons in the riser.

The focus of this study is on the riser reactor, which can be qualitatively divided into three zones as drawn in Figure 1. Zones 1, 2, and 3 are labeled as feed injection, dense phase, and dilute phase, respectively. With the high-activity of modern catalysts, FCC risers have very short contact times. The majority of the cracking and catalyst deactivation occurs in zone 2 where the temperature and catalyst-to-oil ratio are high. Much effort has been expended on the design of feed nozzles and improvement on injection zone mixing and dispersion. While it is desirable to generate small oil drops for fast vaporization, too small drops may lack enough momentum to penetrate far into the riser center zone, thus, wasting the catalyst there.

Correspondence concerning this article should be addressed to C. Zhu at chao.zhu@njit.edu.
Current Address of R. Patel: School of Technology, Pandit Deendayal Petroleum University, Raisan, Gandhinagar, Gujarat 382007, India.

FCC units are designed to crack a wide variety of refinery feedstocks under various conditions. It is essential that an FCC process model can capture the dominant features of kinetics-hydrodynamics interactions, so it can be used for extrapolation purposes. Also, the model should be able to predict product yields, composition, and quality. It is, thus, important to develop robust models based on feedstock composition. Such models allow refiners to take full advantage of recent advances in analytical chemistry, computing, instrumentation, and control. An example of such a composition-based model contains over 3,000 chemical species and 30,000 reactions.[1] The energy industry takes advantage of economies of scale. Hence, even a small change in product slate has a significant impact on economics, making predictive modeling even more important.

In a previous study[2] we developed an FCC riser model that quantifies interactions between hydrodynamics and cracking kinetics—with emphasis on the dense—phase zone (zone 2), where catalyst-catalyst collision plays a key role. The model is represented by a set of first-order ordinary differential equations, and, therefore, can accommodate a large number of reacting species (hence, an even larger number of reactions). As such, this one-dimensional (1-D) model is ideally suited for molecule-based modeling, product differentiation, real-time optimization, online monitoring and control, feedstock selection, and plant monitoring. This stands in sharp contrast to computational-fluid-dynamics-based multidimensional models in which the number of reactions is quite limited. Advancing the hydrodynamic capabilities of existing 1-D models to a higher level has been our strategy for modeling the FCC process. We did so for zone 2 previously[2] and now turn our attention to zone 1 in this study.

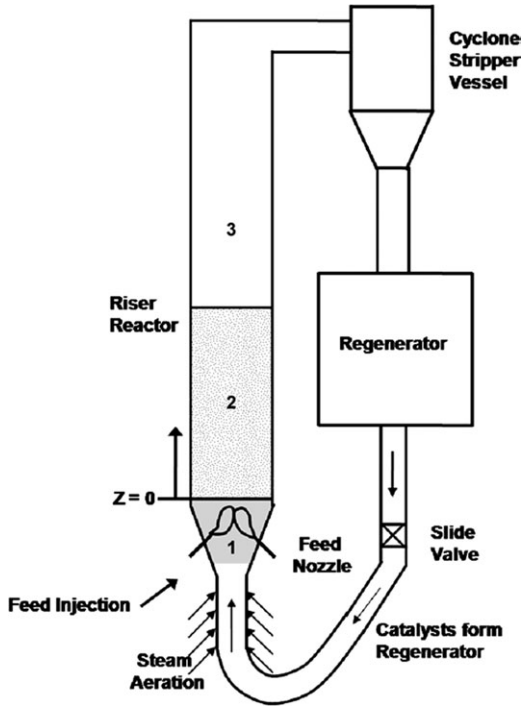

Figure 1. Schematic diagram of an FCC riser reactor.

Most prior FCC models overlook catalytic cracking in the feed injection zone. The underlying assumption has been that the cracking time scale is much longer than the time scale of interfacial transport in the injection zone. So the liquid spray "instantaneously" vaporizes and reaches a thermal equilibrium state with the surrounding medium before cracking sets in. From an overall energy balance, one then calculates an overall catalyst volume fraction and an average gas velocity, which are used as the inlet condition ($z = 0$ in Figure 1) for cracking in the main part of the riser (zones 2 and 3 in Figure 1).

Reasonable as the aforementioned approach may seem, whether precracking in the injection zone can be ignored with impunity remains an open question. In FCC it is impossible for any oil drop to avoid colliding with catalyst even though the droplet volume fraction is very low.[3] Within the injection zone, there are many interacting physicochemical subprocesses (spray deflection, penetration, vaporization, etc.) that are governed by droplet-catalyst collision. Given the high temperature and high-catalyst density in this zone, it is not unreasonable to expect that highly reactive species start to crack.

In light of the above, the present study, and building on our previous work,[2] aims to examine the extent of precracking in the injection zone and its impact on the overall conversion and selectivity. Specifically, we present an elementary model for a quantitative analysis of the physicochemical events taking place in the injection zone. The model captures some salient features of the coupling between interfacial (momentum, heat, and mass) transport and cracking reactions in this zone. Among them are solids and gas entrainments, spray penetration trajectory, droplet-catalyst collision, droplet vaporization, transition from a vapor–liquid–solid flow to a vapor-solid flow, interactions of multiple sprays, and a four-lump cracking kinetic network.

The article's layout consists of an analysis of the spray generated from a single plain circular nozzle, followed by modeling of multiple nozzles using a superposition approach, and last calculation results. It is found that precracking in the injection zone plays an important role in steering the FCC product slate.

Overview of Prior Work

While the literature on FCC research and development is vast, to the best of our knowledge, very little modeling or experimental work has been done on the impact of precracking in the injection zone on FCC riser performance. Here we present a brief review of some relevant prior studies. Several studies were conducted to gain a better understanding of the hydrodynamics of a single- or multiphase jet discharged into gas-only or fluidized gas–solid flow in the absence of chemical reactions. These studies discussed gas and solid entrainment characteristics of single-phase gaseous jets into gas–solid fluidized beds[4–6] or gas-liquid spray jets into gaseous media.[7–9] There are several studies of the effects of droplet-particle collisions on spray penetration and vaporization in fluidized gas–solid flows: laboratory-scale experiments,[10,11] empirical or fundamental modeling,[12–18] and full-field numerical simulation.[19,20] A number of investigators studied the impact of feed injection design on FCC product yields (e.g., gasoline, light fuel oil, etc.). They examined such effects as injector geometry,[21] atomization,[22,23] and spray injection parameters.[24,25] All these prior studies developed multidimensional models based on computational fluid dynamics. As a result, the numbers of reacting species and reactions are necessarily small. Moreover, none of these studies considered systems in which vaporization, spray penetration, and cracking are interactively governed by droplet-catalyst collision.

Here we use a simple four-lump kinetic model[26] to illustrate how we further enhance the hydrodynamic capability of a 1-D riser model developed previously.[2] As Figure 2 shows, vacuum gas oil (VGO) is simultaneously cracked into gasoline, light gases, and coke. These primary reactions are second-order. Due to the high temperatures (e.g., 700–900°K) used, gasoline is further cracked to coke and gases. These secondary reactions are first-order, the gravimetric rate constants of which have the units of g oil/s/g cat. Here k_i ($i = 1 - 5$) are taken as intrinsic rate constants.

Single Spray Injected into Unbounded Cross-flow of Hot Catalyst

Referring to Figure 3a, we consider a plain-orifice atomizer that injects a compact, uniform spray at an angle into an unbounded cross-flow of hot catalyst particles (open circles in Figure 3a). The temperature of the catalyst is far higher than the boiling point of the heaviest component of the oil drop (filled circles). The collision between the high-velocity liquid jet and the flow of massive catalyst particles promotes intense momentum and heat transfer, leading to bending of the spray, vaporization of the drops, and cracking of reactive

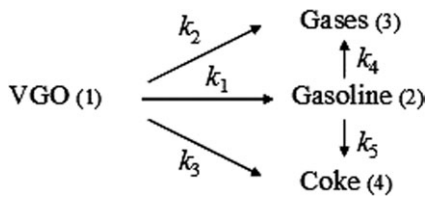

Figure 2. Four-lump catalytic cracking network.

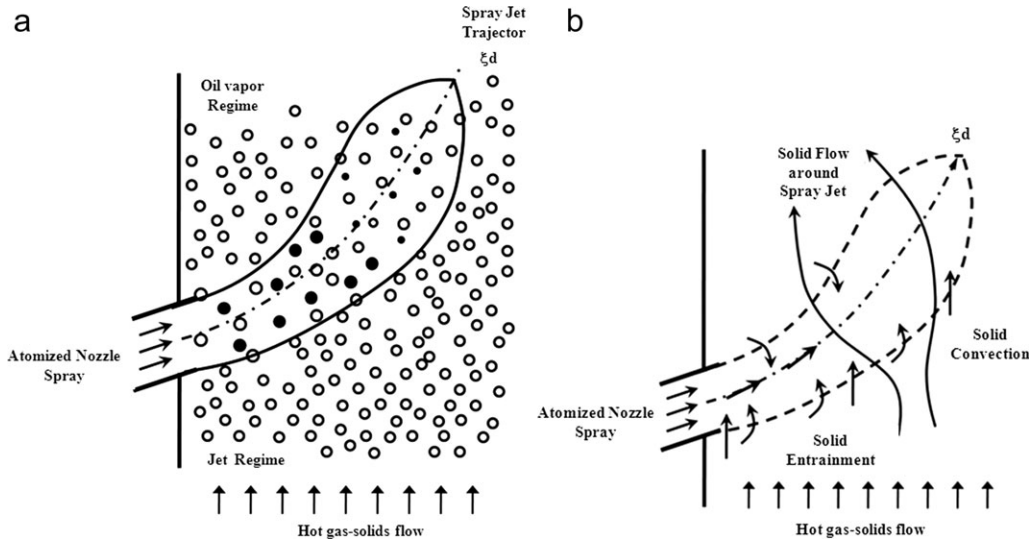

Figure 3. Spray injection into cross-flow of hot catalyst: (a) spray in gas-solid flow, and (b) ambient solid flow.

hydrocarbon species. During the flight from the nozzle exit toward the riser center, the drop's surface decrease can be estimated by the classical D^2-law where D is the drop diameter.[27] The hydrocarbon vapor flows both radially and axially, as shown in Figure 3a. Figure 3b depicts that the catalysts inside the spray region come either from the vapor-jet entrainment or from the particle convective flow. Note also that the catalyst particles can flow through as well as passing around the spray region. Thus, we deal with a system involving interphase transport accompanied by cracking in a vaporizing gas–solid–liquid flow governed by drop-catalyst collision. To develop as simple a model as possible and capture most of the dominant features of the system, we make the following assumptions. (1) The adiabatic riser is at a quasi-steady state, (2) the spray is symmetric, (3) catalyst entrainment in the spray region is driven by the gas jet, (4) a local thermal equilibrium between hot particles and gas phase is quickly established outside the spray region, (5) drop-size variation can be represented by an average drop size, (6) thermophysical properties are constants, (7) heat transfers by radiation and natural convection are negligible, (8) the same catalyst deactivation function can be used for all reactions, and (9) hydrocarbon vapors and steam behave like an ideal gas.

Governing equations

Referring to Figure 4a, we use a deterministic Lagrangian trajectory approach to develop the governing conservation equations for the three-phase flow in a (ξ, η) coordinate system along the spray's centerline.[18] The spray is injected at an angle θ to the horizontal into an unbounded cross-flow of hot catalyst. The derivation of the conservation equations in the (ξ, η) coordinate system is detailed elsewhere,[28] which was an extension of the treatment for a nonreacting system.[18] The general forms of the mass, momentum, and energy balance equations over a control volume in each phase are of the following form[28]

$$\frac{d}{d\xi}(\alpha_i \rho_i u_i A \phi_i) = S_{\phi i} + S_1 \tag{1}$$

When the index i takes on the "values" g, d, and s, the corresponding phases are gas, liquid (droplet), and solid,

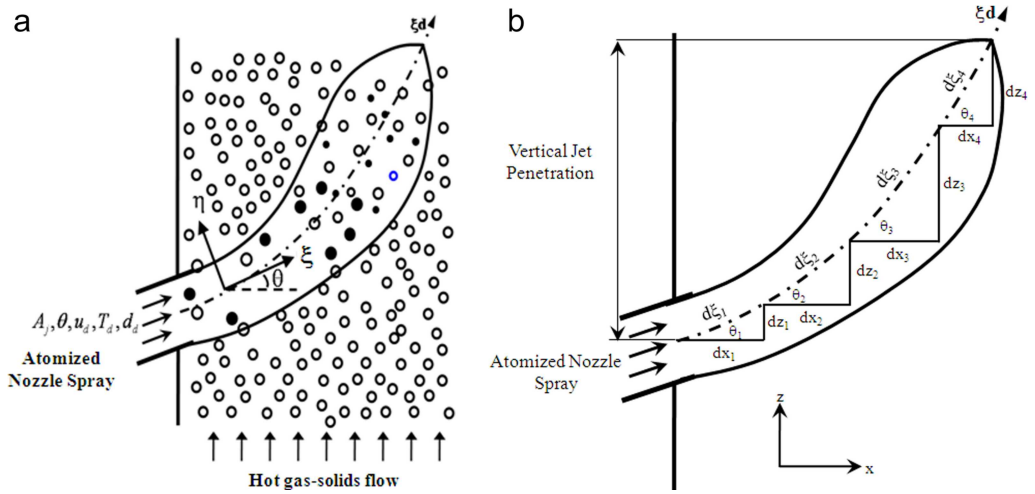

Figure 4. (a) Coordinate system used for tracking spray trajectory, (b) conversion of ξ-coordinate to z-coordinate.

[Color figure can be viewed in the online issue, which is available at wileyonlinelibrary.com.]

Table 1. Definitions of ϕ_i and Source Terms in Eqs. 1 and 2[28]

Phase	Equation	ϕ_i	$S_{\phi i}$	S_I
Gas	Continuity	1	$\dot{m}_{ge}l - \gamma\alpha_g\rho_g u_g l$	$\dot{m}_v A$
	ξ - Momentum	u_g	$\dot{m}_{ge}u_{g\infty}l\cos\theta - \gamma\,\alpha_g\rho_g u_g^2 l$	$\dot{m}_v u_d A - (F_{Dd} + F_{Ds})A$
	Energy	$c_{pg}T_g$	$\dot{m}_{ge}lC_{pg}T_\infty - \gamma\alpha_g\rho_g u_g C_{pg}T_g l$	$\dot{m}_v LA + (E_{Cs} - E_{Cd})A - E_R$
Liquid	Continuity	1	$-\dot{m}_v A$	0
	ξ - Momentum	u_d	$-\dot{m}_v u_d A$	$(F_{Dd} - F_{Cds})A$
	η - Momentum	-	$\dfrac{n_d\left(3\pi\mu d_d u_{g\infty}\sin\theta\right)}{\left(\alpha_g\rho_g u_g^2 + \alpha_d\rho_d u_d^2 + \alpha_s\rho_s u_s^2\right)}$	$\dfrac{\alpha_{s\infty}\rho_s(u_{s\infty}\sin\theta)^2 l}{\left(\alpha_g\rho_g u_g^3 + \alpha_d\rho_d u_d^3 + \alpha_s\rho_s u_s^3\right)A}$
	Energy	$c_{pd}T_d$	$-\dot{m}_v L.A$	$E_{Cds} + E_{Cd}$
Solid	Continuity	1	$\dot{m}_{se}l + \dot{m}_{sp}l$	0
	ξ - Momentum	u_s	$(\dot{m}_{se}l + \dot{m}_{sp}l)u_{se}\cos\theta$	$(F_{Ds} + F_{Cds})A$
	Energy	$c_{ps}T_s$	$(\dot{m}_{se}l + \dot{m}_{sp}l)C_{ps}T_\infty$	$-E_{Cds} - E_{cs}$

respectively. The expressions for ϕ_i,$S_{\phi i}$ and S_i are shown in Table 1 in which momentum terms in the η- and ξ-directions are associated with sinθ and cosθ, respectively. The physical meanings of the symbols are listed in the nomenclature section. The ambient flow conditions are denoted by the subscript ∞. The bending of the spray, described by the η-component of the spray momentum, is mainly caused by the collision between the spray and the upward flow of hot catalyst as well as by the gas drag on the spray. The deflection of the spray in the ξ-direction can be expressed by the ratio of η-component momentum to its total momentum. This leads to the following equation for the variation of θ along the ξ direction

$$\frac{d\theta}{d\xi} = S_{\phi i} + S_1 \tag{2}$$

where the first term on the righthand side represents the effect of drag force on jet bending. The second term represents the momentum increase in the η-direction by the droplet-catalyst collision arising from the cross-flow of catalyst into the spray. Figure 4b shows how the (ξ, η) coordinate for the spray is used to calculate the height of the spray penetration in the z-coordinate (riser).

In FCC riser reactors, steam is injected upstream of the feed injection zone to help disperse the catalyst. The effect of steam on cracking kinetics can be neglected. Based on the four-lump kinetic model, the molar concentration balance equations for each chemical lump as well as steam can be written as follows

$$\frac{d}{d\xi}\left(C_j u_g A\right) = \Gamma_{1j}\Phi_s A + \Gamma_{2j}\Phi_s A + \Gamma_{3j} \tag{3}$$

where Φ_s is the catalyst deactivation function due to coke deposition on the catalyst surface.[29] Where the index j takes on the "values" 1, 2, 3, 4, and 5, the corresponding species are VGO, gasoline, light gases, coke, and steam, respectively. The expressions for Γ_{1j}, Γ_{2j}, and Γ_{3j}, are listed in Table 2.

The gas density of the vapor mixture can be obtained based on the ideal gas law

$$\rho_g = \frac{P}{RT_g}\frac{\sum_{j=1}^{5}\left(C_j M_j\right)}{\sum_{j=1}^{5} C_j} \tag{4}$$

The volume fractions of the three phases are constrained by

$$\alpha_s + \alpha_g + \alpha_d = 1 \tag{5}$$

Note that the ambient flow conditions are denoted by the subscript ∞ in Tables 1 and 2.

Note that Eqs. 1 and 2 together comprise 10 equations governing the hydrodynamics of the three-phase flow. Equation 3 comprises five equations accounting for cracking reactions and catalyst deactivation. With Eqs. 4 and 5, we have 17 coupled governing equations for 17 independent variables (θ, u_g, α_g, T_g, u_d, α_d, T_d, u_s, α_s, T_s, C_1, C_2, C_3, C_4, C_5, ρ_g, and A).

Correlations and constitutive relations

To complete the problem statement, we need to supplement the aforementioned equations with constitutive relations and correlations for various physicochemical subprocesses (e.g., vapor flow induced by ambient convective flow and spray penetration). The volume of catalyst within the spray is governed by the combined actions of entrainment by the spray, vapor-driven acceleration along the spray trajectory, and the convective flow of catalyst outside the spray. Tables 3a and 3b list various correlations and constitutive relations that are derived mechanistically, empirically, or phenomenologically. The details of the correlations and other supplementary information can be found elsewhere.[28]

In Table 3a C/O is the local catalyst-to-oil ratio along the spray jet, while the pre-exponential factor $\bar{k}_{io}$ is molar-based, which can be expressed in terms of mass-based pre-exponential factors k_{io}.[2] Note that a portion of the gas-vapor mixture will leave the spray region as a result of the strong convective cross-flow of the ambient gas–solid mixture. The extent of this outflow, measured by a dimensionless number denoted by γ, depends on the momentum ratio of the cross-

Table 2. Coefficients for Eq. 3[28]

Lump	Γ_{1j}	Γ_{2j}	Γ_{3j}
VGO	$-(k_1 + k_2 + k_3)C_1^2$	0	$\dfrac{\dot{m}_v A}{M_1} - \gamma C_1 u_g l$
Gasoline	$\dfrac{M_1}{M_2}k_1 C_1^2$	$-(k_4 + k_5)C_2$	$-\gamma C_2 u_g l$
Light Gases	$\dfrac{M_1}{M_3}k_2 C_1^2$	$\dfrac{M_2}{M_3}k_4 C_2$	$-\gamma C_3 u_g l$
Coke	$\dfrac{M_1}{M_4}k_3 C_1^2$	$\dfrac{M_2}{M_4}k_5 C_2$	$-\gamma C_4 u_g l$
Steam	0	0	$\dfrac{\dot{m}_{ge} l}{M_5} - \gamma C_5 u_g l$

Table 3a. Constitutive Relations and Correlations[28]

Physical meaning	Symbol	Expression
Drag force	F_{Di}	$n_i c_{Di} \frac{\pi}{8} d_i^2 \rho_g \lvert u_g - u_i \rvert (u_g - u_i)$ $i = d, s$
Collision momentum transfer	F_{Cds}	$f_{ds} \frac{m_s m_d}{(m_s + m_d)} (u_d - u_s)$
Collision frequency[30]	f_{ds}	$\eta_{co} n_d n_s \frac{\pi (d_s + d_d)^2}{4} \lvert u_s - u_d \rvert$
Collision efficiency[17]	η_{co}	$\eta_{co} = \left(1 + 34 \frac{d_d}{d_s} \frac{\rho}{\rho_s} \frac{1}{\mathrm{Re}_{sd}}\right)^{-2}$
Collision heat transfer	E_{Cds}	$f_{ds} \frac{\pi}{6} d_s^3 \rho_s C_{p,s} (T_s - T_d)$
Reaction heat	E_R	$-\sum_{i=1}^{5} r_i . \Delta H_i A$
Heat convection	E_{ci}	$n_i \pi d_i^2 h_i (T_g - T_i)$ $i = d, s$
Heat transfer coefficient	h_i	$h_i = \frac{Nu_i K}{d_i}$ $i = d, s$
Nusselt number for evaporating droplet[31]	Nu_d	$\frac{2 + 0.6 \mathrm{Re}_d^{*0.5} \mathrm{Pr}^{0.333}}{\left[1 + \frac{C_p (T_g - T_d)}{L}\right]^{0.7}}$
Nusselt number for particle[32]	Nu_s	$2 + 0.6 \mathrm{Re}_s^{0.5} \mathrm{Pr}^{0.333}$
Reaction rate Constant	k_i	$k_i = \bar{k}_{i0} \left(\frac{C}{O}\right) exp\left(-\frac{E_i}{RT_i}\right)$

flow to the spray flow. This is expressed as a power law with an exponent n as follows

$$\gamma = \left(\frac{\alpha_{s\infty} \rho_s u_{s\infty}^2 + \alpha_{g\infty} \rho_g u_{g\infty}^2}{\alpha_s \rho_s u_s^2 + \alpha_g \rho_g u_g^2 + \alpha_d \rho_d u_d^2} \right)^n \tag{6}$$

The value of n varies from 0 to 1. We set $n = 0.75$ in this study.

The cracking reaction in an FCC unit starts as soon as the feed vaporizes, so modeling of the droplet vaporization is very important. The energy received by the droplet is mostly consumed by sensible heating and vaporization. Hence, the droplet vaporization rate $\dot{m}_v$ can be calculated by

$$\dot{m}_v = \chi_v \frac{E_{cds} + E_{cs}}{L} \tag{7}$$

where

$$\chi_v = \frac{L}{L + C_{pd}(T_{bd} - T_b)} \tag{8}$$

The mass flux of particles penetrated into the spray jet region depends on a momentum ratio as follows

$$\dot{m}_{sp} = \alpha_{s\infty} \rho_s u_{s\infty} \sin\theta \exp\left(- \frac{\alpha_{s\infty} \rho_s (u_{s\infty} \sin\theta)^2}{\alpha_s \rho_s u_s^2 + \alpha_g \rho_g u_g^2 + \alpha_d \rho_d u_d^2} \right) \tag{9}$$

The term in the denominator represents the momentum of the jet flow, whereas that in the numerator represents the momentum of the ambient particles flowing into the fluidized bed perpendicular to the jet.

Table 3b. Empirical Correlations[12]

Item	Symbol	Correlation
Gas or solid entrainment	$\dot{m}_{ge}, \dot{m}_{se}$	$\alpha_{i\infty} \rho_{g\infty} [0.06(u_i - u_{i\infty} \cos\theta) + 0.3 u_{i\infty} (\cos\theta - \cos\theta_0)]$ $i = d, s$

Interaction of Two Feed Nozzles

A prominent feature of the feed injection zone in a commercial FCC riser reactor is the interactions of multiple sprays. Referring to Figures 5a and 5b, here we consider two symmetric sprays as an example to illustrate how the interactions of multiple sprays are treated. From modeling purposes, the feed injection zone can be qualitatively divided into three regions shown as the shaded area in Figure 5a. In region I, the two sprays do not interact with each other, whereas they become overlapped in region II. The vapor passing through region III contains no oil drops. The vapor flow in region III is driven by the convection of ambient catalyst particles; here the extent of cracking is taken into account in the model, as will be seen later. The vaporization and cracking of the feed lead to cooling, volume expansion, and acceleration of both catalyst and hydrocarbons. As a result, the ambient flow conditions undergo significant changes in this region. As such, the concentrations, velocities, and temperatures of ambient catalyst and vapor-gas mixture must be determined from solving the jet-interaction equations.

Figure 5b shows a simple model for studying transport-reaction coupling in region III. It consists of a number of "microrisers" evenly distributed along the spray path. The transport-reaction processes in each microriser are modeled using the approach developed previously.[2] The same is true for modeling the flow and reaction in the spray-overlapped region. The details of this approach are available

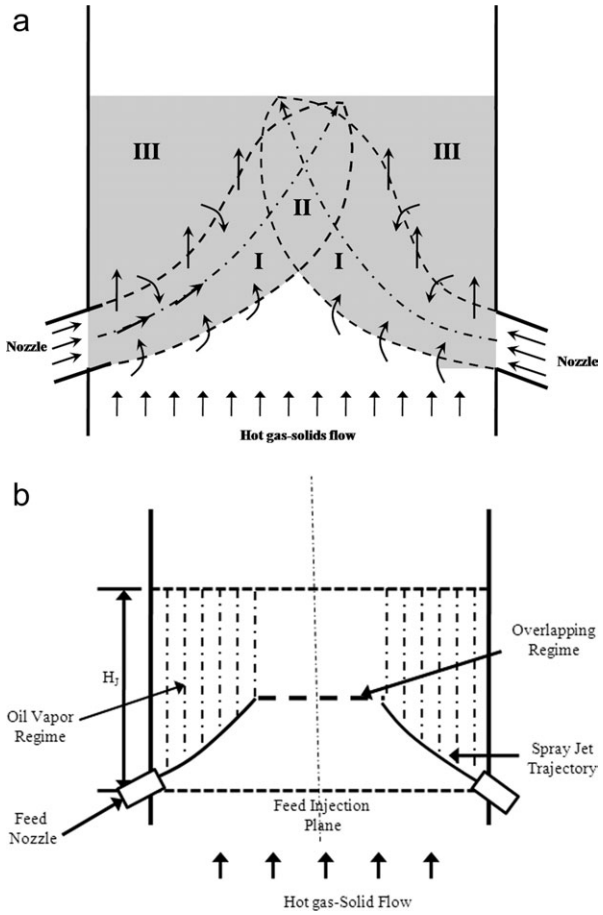

Figure 5. Interactions of two symmetric sprays: (a) shaded area represents the feed injection zone, (b) Multimicroriser model for region III.

Table 4a. Operating Parameters and Thermophysical Constants

Parameter	Value
Catalyst feed rate (kg/s)	192
VGO feed rate (kg/s)/Catalyst flow rate (C/O)	25.2/7.6
Riser diameter (m)	1.0
Riser height (m)	35
Riser inlet temperature (K)	925
Inlet riser pressure (atm)	3.15
Number of nozzles	8
Nozzle radius (mm)	15
Nozzle injection angle (degree)	30
Gaseous jet velocity (m/s)	53
Gas thermal conductivity (w/m K)	0.0415
Gas viscosity (Pa s)	5e-5
Gas thermal capacity (J/kg K)	2250
Crude oil molecular weight (kg/kmol)	400
Gasoline molecular weight (kg/kmol)	108
Light gases molecular weight (kg/kmol)	28
Coke molecular weight (kg/kmol)	32
Steam molecular weight (kg/kmol)	18
Droplet volume fraction at injection	0.0764
Droplet velocity at injection (m/s)	35
Droplet temperature at injection (K)	350
Droplet size at injection (μm)	100
Droplet density (kg/m^3)	900
Droplet saturated temperature (K)	425
Droplet latent heat (J/kg)	220160
Droplet thermal capacity (J/kg K)	2093
Solids (catalyst) size (μm)	75
Solids thermal capacity (J/kg K)	1214
Solids bulk density (kg/m^3)	1400
Solids volume fraction at riser inlet	0.35
Steam velocity at riser inlet (m/s)	1.7

elsewhere,[28] so we do not dwell on them here except to show how an average field variable (concentration, velocity, etc.) at the end of feed injection zone is calculated. Let $\overline{\phi}$ be a field variable obtained from averaging over the riser cross-sectional area. We then have

$$\bar{\phi} = \frac{\phi_0 A_0 + \phi_\infty A_\infty + x\sum_{i=1}^{m} \phi_{ci} A_{ci}}{A_R} \tag{10}$$

Where A_R is the riser cross-sectional area, m the number of microrisers, and x the number of nozzles. The subscripts ∞, 0 and c represent the ambient, overlapping, and microriser regions, respectively. The results obtained in this section are used as the inlet conditions for solving the governing transport-reaction equations for the remaining part of the riser (combined zones 2 and 3 in Figure 1).

Case Study: Results and Discussion

With the modeling framework developed perviously, we are now in a position to ascertain how the feed zone hydrodynamics and reaction affect the riser performance.

Table 4b. Parameters of Four-Lump Kinetic Model[33]

Cracking Reaction	ΔH_i, kJ/kg	k_{io}, g oil/(s· g cat)	E, kJ/kmol
VGO → Gasoline	195	1457.5	57359
VGO → Light Gases	670	127.59	52754
VGO → Coke	745	1.98	31830
Gasoline → Light Gases	530	256.81	65733
Gasoline → Coke	690	0.022	66570

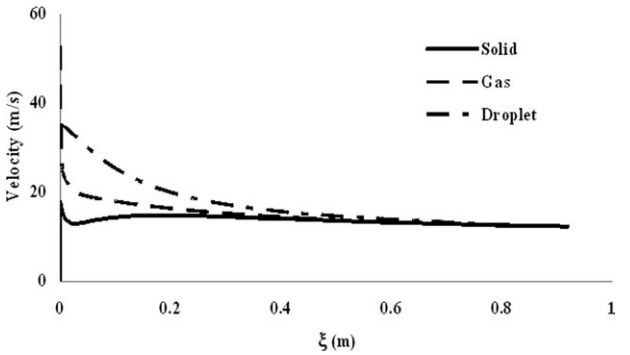

Figure 6. Solid, gas, and droplet velocities along the spray trajectory.

Operating conditions and system parameters

The riser inlet conditions used here are comparable to those used in commercial FCC units. The regenerated catalysts are fed to the riser through a J-bend with steam aeration (Figure 1). The FCC feedstock considered is a typical VGO. Table 4a lists the values of operating parameters and thermophysical constants, while Table 4b lists kinetic constants.

Transport and reaction characteristics of a single feed spray

To validate our model, it would be ideal to have experimental data on vaporizing spray with cracking reactions in a fluidized bed of catalysts. However, to the best of our knowledge, no such data are available in the open literature. Notwithstanding this, we point out that our hydrodynamic model of a vaporizing spray has been validated against experimental measurements in a nonreacting fluidized bed.[34] In what follows we consider a single spray penetrating into an unbounded flow of catalyst. The main task is to quantify the extent of cracking inside the spray. To this end, we need to calculate catalyst concentration, penetration length (hence, oil residence time), and temperature inside the spray. The results will be used to investigate the behavior of multiple jets in the injection zone.

Figures 6 and 7 show the profiles of velocities and volume fractions of the solid, gas, and droplet phases in the spray region, respectively. As can be seen from Figure 6, both gas and droplet velocities decrease along the spray trajectory, which can be attributed to the catalyst entrainment by the spray and the momentum transfer to the catalyst via drag force and droplet-particle collision. Due to droplet's higher

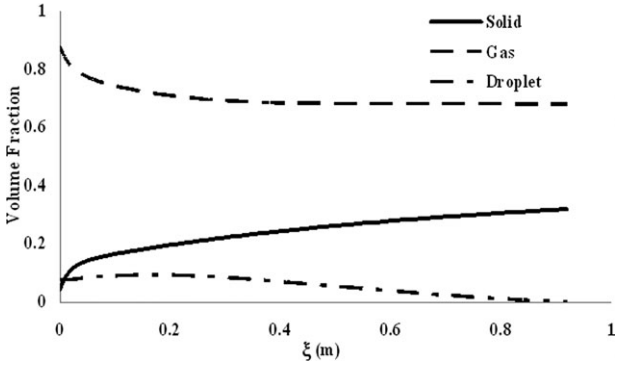

Figure 7. Solid, gas, and droplet volume fractions along the spray trajectory.

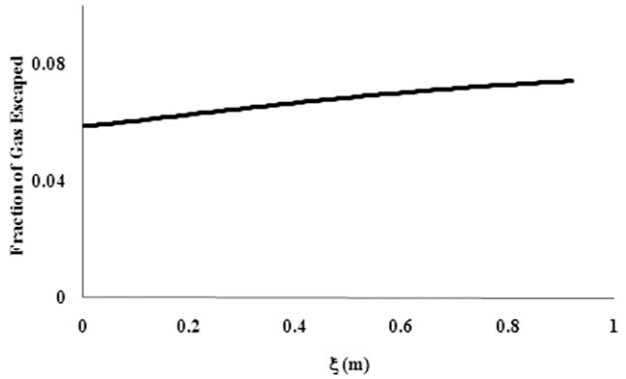

Figure 8. Fraction of gas escaped from the spray region driven by convection of ambient gas solid flow.

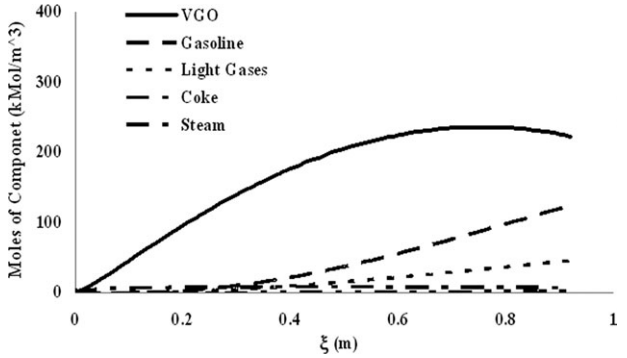

Figure 10. Vapor molar concentrations of FCC chemical lumps in the spray region.

inertia, the droplet velocity decreases more slowly than the gas velocity. The solid velocity, after an initial dip due to entrainment and solid-droplet collision, gradually increases due to the momentum gain from the gas and droplet phases. The system asymptotically reaches an equilibrium state where all three phases have the same velocity. With the intense vaporization and jet expansion, the droplet volume fraction diminishes along the spray trajectory, as Figure 7 shows. The increase in solid volume fraction is attributable to the jet entrainment (especially in the initial jet region), and the enhanced convection driven by the ambient catalyst flow. The solid volume fraction approaches its ambient level at the end of the spray region. While the gas volume is expected to increase rapidly due to droplet vaporization and cracking, some of the gas was drawn out of the spray region by the strong convection of ambient gas–solid flow, as Figure 8 shows. Due to the increased solid volume fraction and the diminishing droplet volume fraction, the gas volume fraction in the spray region asymptotically reaches its ambient value, as displayed in Figure 6.

Figure 9 depicts the solid and gas temperatures along the spray trajectory in the presence and absence of precracking. The initial dip in catalyst temperature (and the corresponding sudden increase in gas temperature) is largely due to the strong, localized solid entrainment by the relatively ''cold'' liquid jet in the vicinity of the nozzle exit. Further decrease in the solid temperature is attributable to liquid vaporization. As Figure 9 shows, the temperature decrease due to endothermic cracking is rather small under the conditions considered. As mentioned earlier, most of the gas is drawn out of the spray region by the convective ambient flow.

The extent of precracking can best be seen by calculating the concentrations of the cracking products in the spray region. Figure 10 plots the gas-phase molar concentrations of the four chemical lumps and steam. As the spray penetrates into the ambient gas–solid flow, the VGO concentration in the gas phase increases due to vaporization and cracking. Figure 10 shows a slow buildup of gasoline; the spray has to travel about 0.4 m before a noticeable amount of gasoline is produced. Here the penetration length is 0.73 m for an injection angle of 30° to the horizontal.

The penetration is defined as vertical distance travelled by the spray jet (height) from the plane of spray injection where the residual mass fraction of liquid feed becomes negligibly small. Figure 11 shows the penetration length as a function of the injection angle. In this case the maximum radial jet penetration occurs at an angle of 35°. Note that here the calculation includes the effect of precracking inside the spray.

Effect of precracking in injection zone on riser performance

The overall effect of the precracking depends on the number of nozzles, their design and spatial arrangement, and the geometry of the riser bottom. The precracking in the injection zone covers the entire shaded area shown in Figure 5a. In what follows we consider eight symmetrical plain, round nozzles installed circumferentially on the reactor wall. Based on the area-average method described earlier, the field variables (e.g., temperature, velocity, etc.) at the end of the injection zone are calculated and listed in Table 5. Here the values of these variables constitute the inlet conditions for a

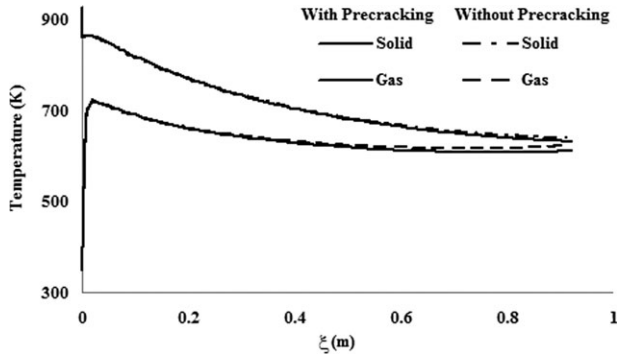

Figure 9. Solid and gas temperatures along the spray trajectory with and without injection zone precracking.

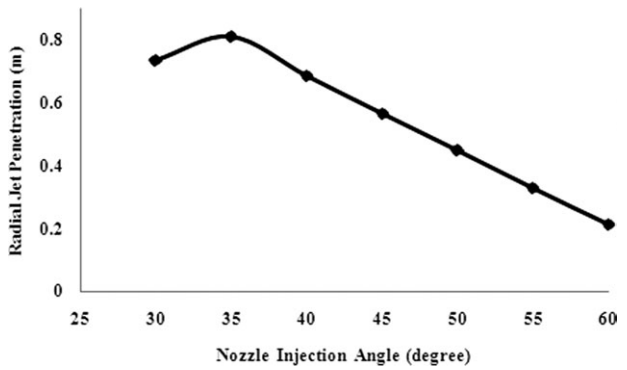

Figure 11. Effect of injection angle on spray penetration length.

Table 5. Average Field Variables Used as Input to an Existing Riser Model[2]

Parameter	Cross-section Average at the End of Injection Zone	
	With Precracking	Without Precracking
Temperature of catalyst (K)	815	827
Solid volume fraction	0.31	0.35
Solid Velocity (m/s)	0.59	0.5
Gas Velocity (m/s)	5.1	2.7
Molar fraction of VGO (%)	69.7	100
Molar fraction of Gasoline (%)	24.25	0
Molar fraction of Light Gases (%)	4.63	0
Molar fraction of Coke (%)	1.42	0
Penetration Length (m)	0.73	0

composition-based FCC riser model developed for cracking in the main section of the riser (combined zones 2 and 3 in Figure 1).[2] Among the distinctive features of the model are the considerations of catalyst-catalyst collision and catalyst-fluid interfacial force.

Using Table 5 as the initial conditions for the aforementioned composition-based riser model,[2] we now assess the impact of injection zone precracking on the overall riser performance. We first look at the gas and solid velocities with and without precracking. These are shown in Figure 12, which plots the velocity profiles downstream of the injection zone (i.e., the riser height here does not include the feed injection zone). As expected, there is a sharp rise in the catalyst velocity in this dense-phase transport and acceleration section (zone 2 in Figure 1). There is also a similar rise in the gas velocity. In either case, the velocity rise is higher in the presence of precracking, as it should be.

Figure 13 shows VGO and gasoline concentration profiles with and without precracking. In the former case, the VGO concentration at the riser outlet is 5% higher than that in the latter case. As a result, the gasoline outlet concentration is 2.3% lower with precracking than without precracking.

The foregoing results can be interpreted as arising from two interlocking events. The differences seen in Figures 12 and 13 are largely attributable to the cracking taking place in zone 2 of Figure 1. The gasoline yield in zone 2 actually is 16% higher with precracking than without precracking. This difference can result in large differences in process economics thanks to the high throughput of the FCC unit, as alluded to earlier. As discussed earlier, the physicochemical events occurring in zone 2 are strongly influenced by the ''initial conditions'' imparted by the injection zone (zone 1).

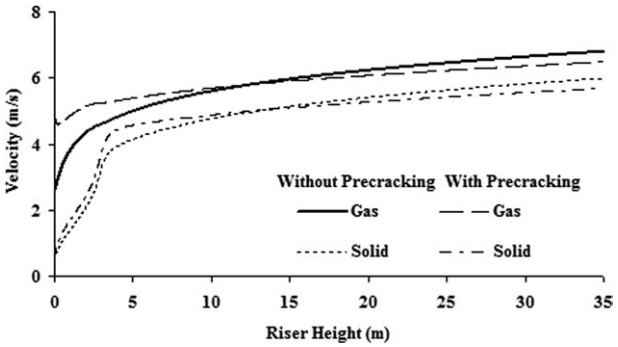

Figure 12. Gas and solid velocity profiles with and without injection zone precracking.

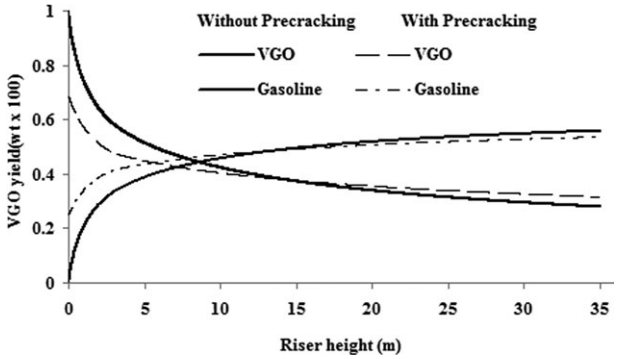

Figure 13. VGO and gsoline concentration profiles with and without feedzone precracking.

This speaks of the importance of injection-zone physics and chemistry for optimal design of an FCC riser. This why there has been a vast patent literatute on the development of new or improved FCC feed injection zone technologies. We next look at a more telling example of the impact of the injection zone.

Selectivity vs. conversion

It is of practical interest to know the relationship between the VGO conversion and the selectivity toward a particular product. The selectivity for gasoline is defined as the ratio of gasoline yield to VGO conversion. To demonstrate the impact of precracking in the injection zone on the gasoline selectivity, we calculate the gasoline selectivity vs. VGO conversion for two cases, as shown in Figure 14.

Figure 14 shows two qualitatively different results. They were obtained by changing only the catalyst inlet temperature and assuming that all VGO liquid droplets instantly vaporized upon colliding with catalyst. The gas–solid equilibrium temperature at the inlet of zone 2 was then calculated by an overall energy balance. The solid curve in Figure 14 is similar to the results shown in Figure 11b of our previous article.[2] With precracking in the injection zone, the gasoline selectivity is higher over a much wider range of VGO conversions. The peak value of the selectivity is slightly reduced, from 80% to about 75%.

The aforementioned results obtained from the four-lump model serve only as an illustrative example. The effect of precracking is expected to be more pronounced had we used a composition-based model that contains tens of thousands of reactions.[1]

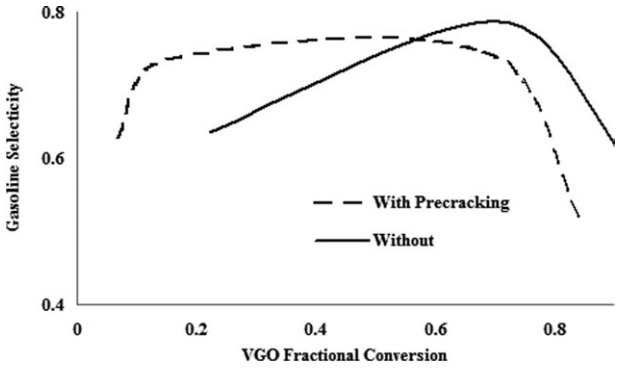

Figure 14. Gasoline selectivity vs. VGO conversion in the presence and absence of injection zone precracking.

Concluding Remarks

Our basic tenet has been that developing a quantitative treatment of the coupling between hydrodynamics and kinetics for 1-D FCC riser models is a pragmatically useful approach to FCC process modeling. Previously, we combined improved momentum equations with the equations of energy and mass to model physicochemical events dominated by catalyst-catalyst collision in the dense-phase zone. In this study, we carry out the task of modeling events dominated by droplet-catalyst collision in the feed injection zone.

Specifically, we in this work developed a simple model that provides a quantitative understanding of the effect of precracking in the feed injection zone on the riser performance. The resulting 1-D model comprises two sets of first-order ordinary differential equations, one for the injection zone and the other for the main part of the riser. As such, the model permits composition-based modeling of real feeds (petroleum fractions, coal liquids, etc.). However, the problem is reduced to that of solving an initial value problem. The ultimate initial condition for the initial value problem is obtained from the treatment developed in this work. With a four-lump cracking kinetic model as an illustrative example, we find that precracking in the injection zone plays an important role in determining the FCC conversion and selectivity. Further work should relax some of the strong assumptions used in this work. For example, to better quantify the effect of precracking on the cumulative yields of products at the riser exit, a core-annulus model with catalyst backmixing near the wall needs to be developed. Future models should also consider such characteristics as drop size distribution, molecule-based cracking kinetics, down flow of spent catalysts near the riser wall, to name just a few.

Notation

A = jet cross-sectional area, m^2
C_j = molar concentration of j^{th} lump, mol/m^3
C_p = specific heat, J/kg K
c_D = drag coefficient
D = diameter, m
E_c = convective heat-transfer rate, J/s
E_R = reaction heat transfer rate, J/s
E_i = activation energy of the i^{th} reaction, kJ/mol
F_D = drag force, N
k_i = rate constant of i^{th} cracking reaction
L = latent heat of vaporization, J/kg
l = jet perimeter
M_j = molecular weight of j^{th} lump, kg/mol
$\dot{m}_{ge}$ = gas entrainment mass flux rate, kg/m^2 s
$\dot{m}_{se}$ = solid entrainment mass flux rate, kg/m^2 s
$\dot{m}_{sp}$ = solid penetration by convection, kg/m^2 s
$\dot{m}_v$ = droplet vaporization rate, kg/m^3 s
n_d = droplet number density, m^{-3}
P = pressure, atm
R = universal gas constant, J/mol K
T = temperature, K
u = velocity, m/s

Greek letters

α = volume fraction of different phases
γ = partition function for vapor convection
θ = spray injection angle, degree
μ = dynamic viscosity of fluid, $N{\cdot}s/m^2$
ρ = density (kg/m^3)
Φ_s = catalyst deactivation coefficient

Subscripts

d = droplet
s = solid
l = liquid
g = gas
b = boiling point
∞ = ambient flow condition

Literature Cited

1. Christensen G, Apelian MR, Hicky KJ, Jaffe SB. Future directions in modeling the FCC process: An emphasis on product quality. *Chem Eng Sci*. 1999;54:2753–2764.
2. Zhu C, Jun Y, Patel R, Wang D, Ho TC. Interactions of flow and reaction in fluid catalytic cracking risers. *AIChE J*. 2011;57(11): 3122–3131.
3. Ho TC. On catalyst-oil interactions in fluid catalytic cracking. *J Chin Inst Chem Eng*. 2006;37(1):25–35.
4. Field MA. Entrainment into an air jet laden with particles. *BCURA Inf*. 1963.
5. Ricou FP, Spalding DB. Measurements of entrainment by axisymmetrical turbulent jets. *J Fluid Mech*. 1961;11(1).
6. Subramanian V, Ganesh R. Influence of free stream velocity on the entrainment by single- and two-phase axisymmetric jet. *AIChE J*. 1984;30(6):1010–1013.
7. Edelman RB, Economos C, Boccio J. Mixing and combustion in two-phase flows with application to the B—O—H—N system. *AIAA J*. 1971;9:1935–1940.
8. Chen TH, Roe LA, Nejad AS. Multifunction droplet imaging and velocimetry system for spray jets. *J Propul Power*. 1994;10(6): 798–803.
9. Wu PK, Kirkendall KA, Fuller RP. Spray structures of liquid jets atomized in subsonic crossfows. *J Propul Power*. 1998;14(2):173–182.
10. Skouby DC. Hydrodynamics studies in a 0.45-m riser with liquid feed injection. In: Proceedings of the 1998 AIChE Annual Meeting; 1998.
11. Zhu C, Wang X, Fan LS. Effect of solids concentration on evaporative liquid jets in gas-solid flows. *Powder Technol*. 2000;111(1–2): 79–82.
12. Platten JL, Keffer JF. Entrainment in Deflected Axisymmetric Jets at Various Angles to the Stream. Dept of Mechanical Engineering. University of Toronto. Technical Report. 1968;6808.
13. Campbell JF, Schetz JA. Flow properties of submerged heated effluents in a waterway. *AIAA J*. 1973;11(2):223–230.
14. Li HS, Karagozian AR. Breakup of a liquid jet in supersonic crossflow. *AIAA J*. 1992;30(7):1919–1921.
15. Han KS, Chung MK. Numerical simulation of a two-phase gas-particle jet in a crossflow. *Aero Sci Technol*. 1992;17(2):59–68.
16. Fan LS, Lau R, Zhu C, Vuong K, Warsito W, Wang X, Liu G. Evaporative liquid jets in gas-liquid-solid flow system. *Chem Eng Sci*. 2001;56:5871–5891.
17. Zhu C, Wang X, Liu G. Fan LS. A similarity model of evaporating liquid spray jets in concurrent gas-solid flows. *Powder Technol*. 2000;119(2–3):292–297.
18. Zhu C, Liu G, Wang X, Fan LS. A parametric model for evaporating liquid jets in dilute gas-solid flows. *Int J Multiphase Flow*. 2002;28:1479–1495.
19. Wang XH, Zhu C, Ahluwalia R. Numerical simulation of evaporating spray jets in concurrent gas-solids pipe flows. *Powder Technol*. 2004;140(1–2):56–67.
20. Qureshi, MMR, Zhu C. Cross-flow evaporating sprays in gas-solid flows: Effect of aspect ratio of rectangular nozzles. *Powder Technol*. 2006;166(2):60–71.
21. Theologos KN, Markatos NC. Advanced modeling of fluid catalytic cracking riser-type reactors. *AIChE J*. 1993;39:1007–1017.
22. Theologos KN, Lygeros AI, Markatos NC. Feedstock atomization effects on FCC riser reactors selectivity. *Chem Eng Sci*. 1999;54(22):5617–5625.
23. Gao JS, Xu, CM, Lin SX, Yang GH, Guo YC. Simulations of gas-liquid-solid 3-phaseflow and reaction in FCC riser reactors. *AIChE J*. 2001;47(3):677–692.
24. Chang SL, Lottes SA, Zhou CQ, Bowman BJ, Petrick M. Numerical study of spray injection effects on the heat transfer and product yields of FCC riser reactors. *J Heat Transfer Trans ASME*. 2001;123(3):544–555.
25. Chang SL, Zhou CQ. Simulation of FCC riser flow with multiphase heat transfer and cracking reactions. *Comput Mech*. 2003;31(6): 519–532.

26. Lee LS, Chen YW, Huang TN, Pan WY. Four-lump kinetic model for fluid catalytic cracking process. *Can J Chem Eng*. 1989;67: 615–619.
27. Huang Z, Ho TC. Effect of thermolysis on resid droplet vaporization in fluid catalytic cracking. *Chem Eng J*. 2003;91:45–58.
28. Patel R. Modeling of Non-Uniform Hydrodynamics and Catalytic Reaction in a Solids-Laden Riser [Ph.D. Thesis]. Mechanical & Industrial Engineering Department, New Jersey Institute of Technology, Newark, NJ; 2011.
29. Pitault I, Nevicato D, Blasetti AP, Delasa HI. Fluid catalytic cracking catalyst for reformulated gasoline-kinetic modeling. *Ind. Eng. Chem. Res*. 1994;33:3053–3062.
30. Fan LS, Zhu C. In: *Principles of Gas-Solid Flows*. Cambridge, UK: Cambridge University Press; 1998;172.
31. Dwyer, HA. Progress energy combustion science. *Combust Sci Technol*. 1985;15:131.
32. Buchanan JS. Analysis of heating and vaporization of feed droplets in fluidized catalytic cracking risers. *Ind Eng Chem Res*. 1994; 33(12):3104–3111.
33. Han IS, Chung CB. Dynamic modeling and simulation of fluidized catalytic cracking process, Part-II: Property estimation and simulation. *Chem Eng Sci*. 2001;56:1973–1990.
34. Wang, D. Transport Mechanisms and Modeling of Riser Reactor [Ph.D. Thesis]. Mechanical & Industrial Engineering Department, New Jersey Institute of Technology, Newark, NJ; 2010.

Manuscript received Apr. 17, 2012, and revision received July 23, 2012.